frontiers | Frontiers in Energy Research

TYPE Original Research
PUBLISHED 11 January 2023
DOI 10.3389/fenrg.2022.1117606

OPEN ACCESS

EDITED BY
Ling Zhou,
Jiangsu University, China

REVIEWED BY
Jiaxing Lu,
Xihua University, China
Hao Yan,
Hefei University of Technology, China
Jinya Zhang,
China University of Petroleum, China

*CORRESPONDENCE
Junzhao Han,
hanjz@zstu.edu.cn

SPECIALTY SECTION
This article was submitted to Process and Energy Systems Engineering, a section of the journal Frontiers in Energy Research

RECEIVED 06 December 2022
ACCEPTED 23 December 2022
PUBLISHED 11 January 2023

CITATION
Pan J, Ma J, Han J, Zhou Y, Wu L and Zhang W (2023), Prediction of sediment wear of francis turbine with high head and high sediment content.
Front. Energy Res. 10:1117606.
doi: 10.3389/fenrg.2022.1117606

Prediction of sediment wear of francis turbine with high head and high sediment content

Jun Pan[1], Jianfeng Ma[1], Junzhao Han[1]*, Ye Zhou[2], Lielong Wu[3] and Weiliang Zhang[1]

[1]Zhejiang Province's Key Laboratory of Reliability Technology for Mechanical and Electronic Product, Zhejiang Sci-Tech University, Hangzhou, China, [2]Department of Operation Support, Institute of Hydraulic Machinery, China Institute of Water Resources and Hydropower Research, Beijing, China, [3]Hangzhou Resource Power Equipment Co.Ltd, Hangzhou, China

Wear of runner blades is a common problem affecting the operational reliability of turbines with high head and high sediment content. In order to accurately predict the wear of the turbine runner blade, based on the solid-liquid two-phase flow equation and turbulence model, the full channel numerical simulation of the internal water and sediment flow was carried out, and the sediment volume distribution and sand water velocity on the turbine runner blade were obtained. Then, according to the digital simulation results and the operating parameters of the turbine runner, the sediment wear test scheme for the turbine blade material specimen is designed, and the sediment wear test is carried out on the runner material. According to the test results, the sediment wear curve of runner blade material is obtained and applied to numerical simulation, and the main position and wear degree of turbine blade sediment erosion are predicted. The inspection results of the runner blade wear after the unit has operated for a flood season show that obvious wear can be seen at the outlet edge of the lower band of the runner blade, and the wear position and wear amount are basically consistent with the simulation values. The study is of great importance for predicting the wear of turbine runner blades with high drop height and high sediment content, and for turbine maintenance under complex conditions.

KEYWORDS

sediment wear, sediment content, complex conditions, francis turbine, wear depth

1 Introduction

Prediction of wear of sand erosion has always been a very important topic in the field of hydraulic machinery. As for the wear mechanism, based on the Euler-Euler method, Zhou et al. (Zhou et al., 2022) numerically simulated the turbine with long and short blades under the condition of sediment-laden water. The results show that the erosion area increases with increasing sediment particle size when the sediment volume fraction is constant. Using experiments and simulations CFD-DEM, Xu et al. (Xu et al., 2022) investigated the influence of the spherical valve arrangement on the two-phase flow and erosion distribution in the valve. The results show that the surface of the eroded plate forms a wavy texture under the condition of a small opening. When the placement method changes from vertical to horizontal, the particle distribution easily accumulates near some walls and forms a protective layer, which reduces the erosion rate. Noon and Kim et al. (Noon and Kim, 2016) performed a three-dimensional numerical analysis of the erosion of lime slurry flowing through a centrifugal pump and its effects on head and loss of efficiency. The results show that the impact velocity, mass concentration and solid particle diameter are crucial for erosion damage. Bohn B et al. (Bohn et al., 2019) have designed and fabricated a magnetic sensor to

measure impeller blade wear during operation of a centrifugal pump. With increasing wear, the impeller gap increases and the total reluctance of the magnetic circuit increases, which leads to a decrease in the peak inductance of the coil. The sensor helps to monitor the wear of the impeller blades. The results show that the geometric changes strongly influence the flow properties and thus affect the erosion mode. Tarodiya et al. (Tarodiya and Gandhi, 2019) used mixed and Euler-Euler multiphase models for multiphase modeling of a centrifugal slurry pump. The results showed that the head and efficiency of the pump decreased with increasing particle size and concentration. In the Euler-Euler model, the liquid (f) and solid (s) phases are assumed to coexist at every point in space in the form of an interpenetrating continuity. By solving the continuity equation and the momentum equation of the two phases, the volume fraction of the liquid phase and the solid phase are obtained, and the coupling between the phases is realized by the exchange coefficient.

Tang et al. (Tang et al., 2021) investigated the effect of particle shape on the wear properties of centrifugal pumps with CFD-DEM. The results show that as the sphericity of the particles increases, the overall pump impact wear first decreases and then increases. The internal impeller impact wear occurs mainly at the leading edge of the blade. Regardless of how the particle shape and wear mode change, the volute is the main wear part. Shi et al. (Shi et al., 2020) performed a numerical study on the internal flow field of a solid-liquid centrifugal pump and used the wear equation to predict the wear of the volute casing due to the solid-liquid two-phase flow. The wear mechanism of the volute casing of a centrifugal pump is analyzed in detail and systematically. The results show that the relative wear along the volute is a function of the erosion behavior of the volute material and the impact angle of the solid particles around the volute. Tao et al. (Tao et al., 2021) investigated the effects of blade thickness on the solid-liquid two-phase flow and impeller wear of a ceramic centrifugal slurry pump by numerical simulation and wear test. As the thickness of the blade increases, the angle of impact of the solid particles increases, which leads to an increase in the angle of wrap of the trajectory of the solid particles. By increasing the wrap angle of the solid particles, the collision area between the pressure side of the blade and the solid particle side is shifted toward the impeller outlet and more collisions occur between the solid particles and the suction side of the blade, which increases the wear of the suction side of the blade.

At present, there are relatively few studies on the prediction of sediment wear on the impeller of the high head hydropower station mixed flow system, and the formation mechanism of flow component wear is still insufficient. Currently published in the relevant literature, according to the hydropower station where the flow sediment combined with runner material in the wear test rig to carry out the test, and through the runner blade running a flood season according to the measured data on the high head mixed flow unit wear characteristics analysis and prediction of the literature is also less, so it is necessary to high head mixed flow unit runner wear in-depth discussion. In this paper, based on the Euler model combined with the turbine wear prediction method proposed by Duronev and Pelaev, the wear characteristics of a high head Francis turbine in a hydropower station are predicted under rated operating conditions. The internal flow characteristics, particle distribution, wear location, and wear prediction of the runner are analyzed in detail, and the performance of the runner against sediment wear is investigated.

2 Three-dimensional model and numerical calculation model

2.1 3D model

The research object is a Francis turbine with high head in a hydropower station. The runner of the high-head turbine consists of 15 long and 15 short blades, an upper crown and a lower band. The 15 long and 15 short blades are staggered and welded to the upper crown and lower band to form a runner body. There are 16 stay vane and 24 guide vane. The sectional view of high-head turbine is show in Figure 1.

The main parameters of high-head turbine are shown in Table 1.

Based on the geometrical parameters of the entire flow channel of the hydraulic turbine, a three-dimensional calculation area for the flow field is defined. The whole calculation area includes five parts: Spiral casing, stay vane, guide vane, hydraulic turbine runner and draft tube. The entire flow channel is shown in Figure 2.

2.2 Finite element model

The three-dimensional model of the Francis turbine with a large drop height is created using the ICEM software and a structured grid. The geometric structure of the spiral casing and the runner is more complex, the geometric size range is large, the flow is complex and the local grid density needs to be increased. The mesh quality is above .5, which meets the requirements of numerical simulation. The models of the entire computational grid and the subcomponents of the computational grid are shown in the following Figure 3.

The computational grid is divided into different number of grids with about 1 million increments. The independence test of the grid is performed with the measured efficiency in the rated operation of the turbine as a control parameter The fourth grid in Table 2 below has an error of less than .2% and meets the requirements for the grid independence detection.

From Table 2, in the absence of sand particles, the relative error between the computational efficiency and the measured efficiency is smallest when the number of grids reaches 10.25 million, so the fourth scheme was selected as the best.

2.3 Boundary condition

The specific boundary conditions are set according to the rated operating condition of the turbine of the hydropower station. Unit operation rated head is H_p = 282 m and rated speed is 500 r/min. According to the hydrological data of the hydropower station some parameters can be determined: the inlet pipe sediment concentration of the hydropower station actual multi-year flood season sediment concentration of 1.93 kg/m^3 (sediment volume fraction of ϕ_g = .00074), median particle size of sediment d = .02 mm. Mean particle size of sediment is used as sand diameter in calculation.

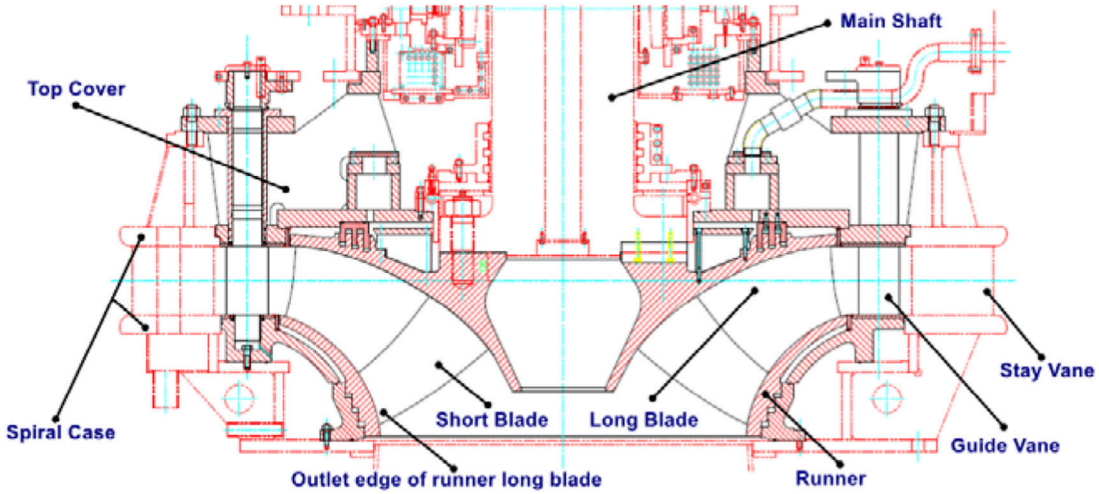

FIGURE 1
The sectional view of high-head turbine.

TABLE 1 Parameters of high head turbine.

Diameter D_1 (mm)	Runner blades number N	Distribution circle diameter of guide vane D_2 (mm)	Guide vane height H_{GV}	Spiral casing inlet diameter D_3 (mm)
2,350	15 long+15 short	2,650	288 mm	580

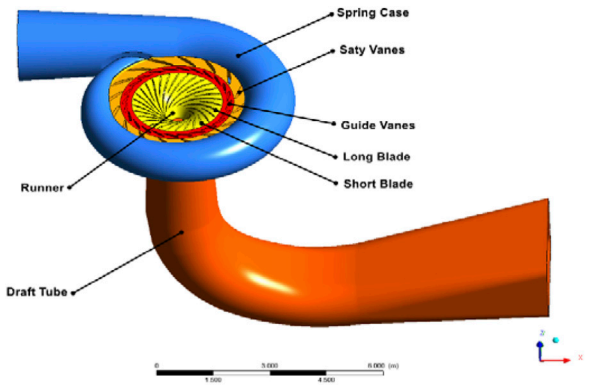

FIGURE 2
The entire flow passage's model of internal water-sediment flow in high-head Francis turbine.

The inlet and outlet boundaries are set at the inlet of the volute and at the outlet of the draft tube. In the case of uniform flow, the total pressure is given at the inlet. In this work, the pressure outlet has a better convergence speed, and the specific data are given according to the design conditions. For the solid wall, the no-slip condition is assumed that the normal velocity is 0. After the single-phase steady-state calculation of each working condition, it is used as the initial condition for the multi-phase calculation range. The dynamic and static interface is given as dynamic and static rotor.

2.4 Governing equation

With the rapid development of high-performance computers and numerical simulation methods, computational fluid dynamics (CFD) has become an effective method for studying complex two-phase flows. In this study, the Euler-Euler model is generally used to simulate multiphase flows (Tian, 2020).

2.4.1 The basic equation of liquid-solid two-phase flow

The motion equation of solid-liquid two-phase flow in Euler coordinate system:

Liquid phase continuity equation can be expressed as:

$$\frac{\partial \phi_f}{\partial t} + \frac{\partial}{\partial x_i}\left(\phi_f U_i\right) = 0$$

Solid phase continuity equation can be expressed as:

$$\frac{\partial \phi_p}{\partial t} + \frac{\partial}{\partial x_i}\left(\phi_p V_i\right) = 0$$

Liquid phase momentum equation can be expressed as:

$$\frac{\partial}{\partial xt}\left(\phi_f U_i\right) + \frac{\partial}{\partial x_k}\left(\phi_f U_i U_k\right) = -\frac{1}{\rho_f}\phi_f \frac{\partial P}{\partial x_i} + \nu_f \frac{\partial}{\partial x_i}\left[\phi_f\left(\frac{\partial U_i}{\partial x_k} + \frac{\partial U_k}{\partial x_i}\right)\right] - \frac{B}{\rho_f}\phi_f \phi_g \left(U_i - V_i\right) + \phi_f g_i$$

Solid phase momentum equation can be expressed as:

10.3389/fenrg.2022.1117606

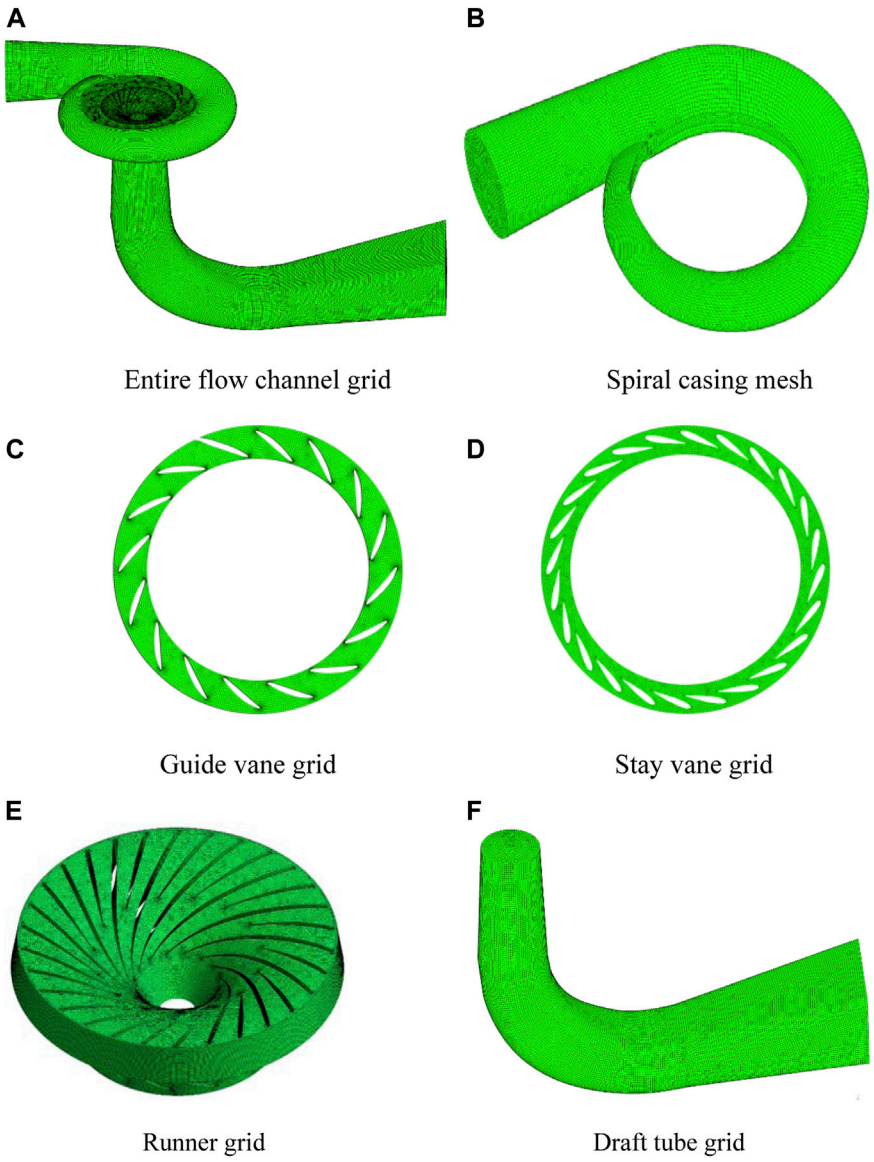

FIGURE 3
Hydraulic turbine grid model. **(A)** Entire flow channel grid **(B)** Spiral casing mesh. **(C)** Guide vane grid **(D)** Stay vane grid. **(E)** Runner grid **(F)** Draft tube grid.

$$\frac{\partial}{\partial t}\left(\phi_g V_i\right)+\frac{\partial}{\partial x_k}\left(\phi_g V_i V_k\right)=-\frac{1}{\rho_g}\phi_g\frac{\partial P}{\partial x_i}+\nu_g\frac{\partial}{\partial x_k}\left[\phi_g\left(\frac{\partial V_i}{\partial x_k}+\frac{\partial V_k}{\partial x_i}\right)\right]-\frac{B}{\rho_g}\phi_f\phi_g\left(V_i-U_i\right)+\phi_g g_i$$

where U_i is the velocity component of the liquid phase, V_i is the velocity component of the solid phase, ρ is density of phase material, ν is the viscosity coefficient of phase material motion, B represents the interphase interaction coefficient, which is related to the flow field parameters such as the Reynolds number of sediment particles, P is the pressure, g is the gravity acceleration, x_i is the coordinate component, d is the sediment diameter; ϕ is phase volume fraction and $\phi_f+\phi_g=1$, f is the subscript indicates the liquid phase, g is the subscript indicates the solid phase.

2.4.2 Turbulent flow model

For the turbine, its internal flow is very full turbulent flow, this paper uses the $k-\varepsilon$ model:

Liquid phase continuity equation can be expressed as:

$$\frac{\partial}{\partial t}\left(\rho k\right)+\frac{\partial}{\partial x_j}\left(\rho v_i k\right)=\frac{\partial}{\partial x_j}\left(\left(\mu+\frac{\mu_t}{\sigma_k}\right)\frac{\partial k}{\partial x_j}\right)+G_k+G_b-\rho\varepsilon-Y_M$$

The continuity equation of sediment particles can be expressed as:

$$\frac{\partial}{\partial t}\left(\rho\varepsilon\right)+\frac{\partial}{\partial x_j}\left(\rho v_i\varepsilon\right)=\frac{\partial}{\partial x_j}\left(\left(\mu+\frac{\mu_t}{\sigma_\varepsilon}\right)\frac{\partial\varepsilon}{\partial x_j}\right)+C_{1\varepsilon}\frac{\varepsilon}{k}\left(G_k+C_{3\varepsilon}G_b\right)-C_{2\varepsilon}\rho\frac{\varepsilon^2}{k}$$

TABLE 2 Grid independence verification.

NO	Grid number N/ million	Computational efficiency of hydraulic turbine (%)	Measured efficiency of hydraulic turbine (%)	Relative error (%)
1	7.50	92.30	95.21	3.05
2	8.42	94.51	95.21	1.79
3	9.36	94.28	95.21	.97
4	10.25	95.02	95.21	.19

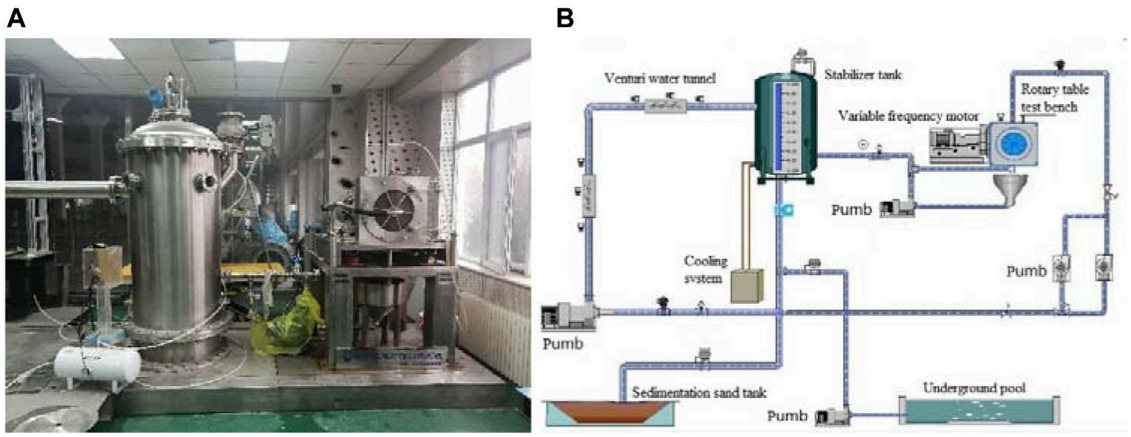

FIGURE 4
(A) Hydraulic machinery abrasion test system **(B)** Testing apparatus scheme.

where, G_b、 Y_M are the turbulent kinetic energy generated by buoyancy and the generation term generated by diffusion in compressible turbulence, respectively, and their specific forms may refer to relevant data; G_k represents the turbulent kinetic energy generation term caused by the average velocity gradient.

3 Sand slurry abrasion test for the specimen

3.1 Experiment equipment

The wear test device uses the hydraulic-mechanical wear test system independently developed by the Institute of Mechanical and Electrical Engineering of the Chinese Academy of Water Sciences. The schematic diagram is shown in Figure 4. The test device mainly consists of a pressure vessel, a rotary table, a variable frequency motor, a water pump, a cooling system, and a measuring device. Six fan-shaped specimens with a front diameter of 400 mm are installed on the rotary table to form a torus, as shown in Figure 4B.

Thus, the experimental principle is to determine the velocity distribution of the sand water around the impeller blade by numerically simulating the sand water flow in the turbine under rated conditions. The flow velocity range of blades is 25 m/s~45 m/s, as shown in the following Figure 5.

Abrasion experiments were conducted based on five groups of overcurrent velocities of 25 m/s, 30 m/s, 35 m/s, 40 m/s and 45 m/s. The sediment conditions and flow velocity on the surface of the sample correspond to the actual flow velocities on the surface of the turbine and runner blades to ensure that the experimental results are consistent with rated condition of hydraulic turbine. The relationship between wear volume per unit time and velocity was determined through several series of experiments at various overflow velocities.

3.2 Specimen

The hydropower station is located in the plateau, 2,200 m above sea level. The average annual sediment concentration is 1.93 kg/m^3 and the average annual suspended sediment mass is 1.74 million tons. According to the hydrological bureau, suspended sediment was sampled in the river near the dam of the hydropower station. The maximum particle size was .535 mm and the mean particle size was .02 mm. Analysis of the mineral composition and content of the sediment. The mineral composition and content of the sediment were determined by X-ray diffraction analysis. The results of the analysis are shown in the following Table 3. The mineral composition of the sediment consists mainly of quartz, feldspar and clay minerals, with the proportion of hard particles with Mohs hardness greater than 5 being 55.6%.

The material of the test specimen corresponds to the material of the turbine blades of a hydroelectric station with high water level The material of the test piece is 0Cr13Ni5Mo. The test piece is shown in Figure 6.

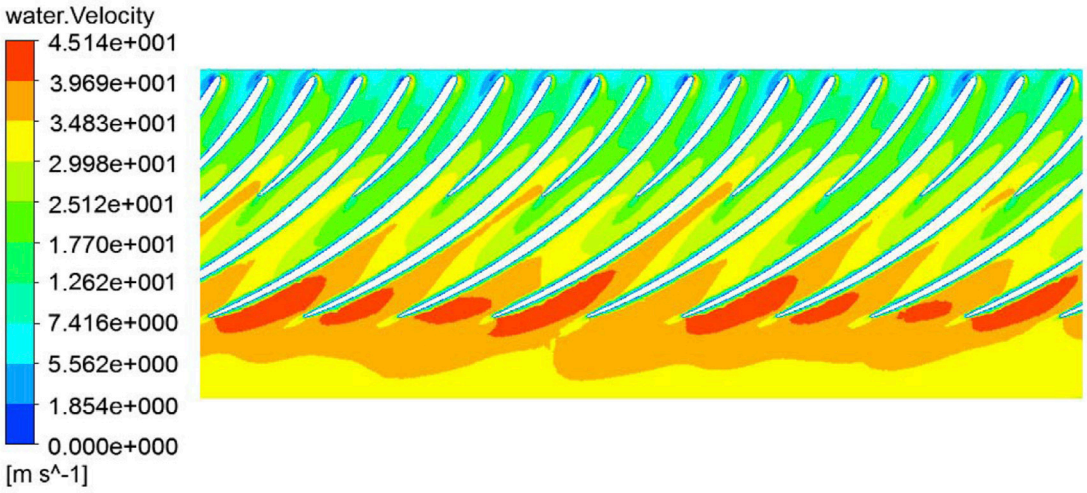

FIGURE 5
Velocity distribution of flowing sand water.

TABLE 3 Mineral composition and content of sediment in power station.

Mineral name	Quartz	Potassium	Feldspar	Albite	Calcite	Dolomite	Illite	Kaolinite	Chlorite
Mineral contents%	43.2	3.3	9.1	4.9	2.8	25.2	3.6	3.9	4
Mineral Mo hardness	7	6	6	3	3–4	2–3	2–3	1–2	—
Hard particle content	55.6%			—	—	Clay minerals			

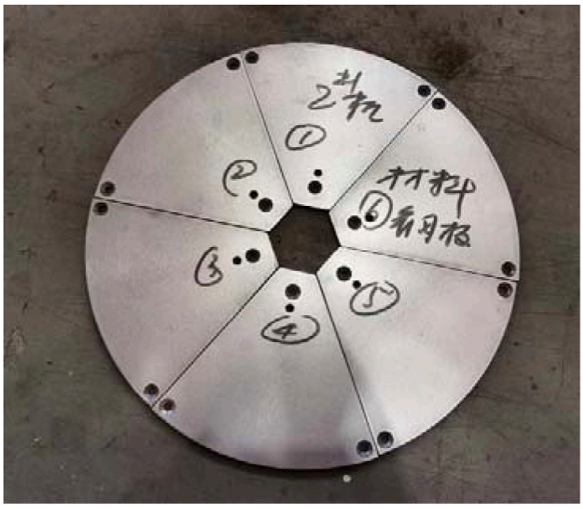

FIGURE 6
Wear test bench specimen.

FIGURE 7
Wear test bench specimen after a period of time (T = 12 h).

3.3 Test results and fitting material test sediment wear curve

According to the method proposed by Durinev and Pelaev for predicting turbine wear, the following relationship can be summarized for the calculation of wear (Yu et al., 2007):

$$\Delta H = K \cdot k_s \cdot S^M \cdot W^N \cdot T$$

where, ΔH is wear depth of material, k_s is influence coefficient of sediment characteristics, K is material performance influence coefficient and the comprehensive influence coefficient of other factors, S is sediment concentration, M is index, W is relative velocity of water flow, N is index, T is time to wear out.

The test material and sediment composition content are consistent with the real hydropower station, and the influence coefficient k_s and sediment concentration index M are about 1.0.

TABLE 4 Relationship between unit wear rate *E* and velocity W.

W (m/s)	25	30	35	40	45	ΔH = K·S.T.W^N	
T(h)	12	12	12	12	12		
S = 1.93 kg/m^3	Wear rate per unit time E (um/h)					K (×10^{-9})	N
Specimen Wear depth ΔH	2.2	4.39	7.8	12.7	19.7	.65	3.70
Unit wear rate E	.183	.365	.65	1.06	1.64		

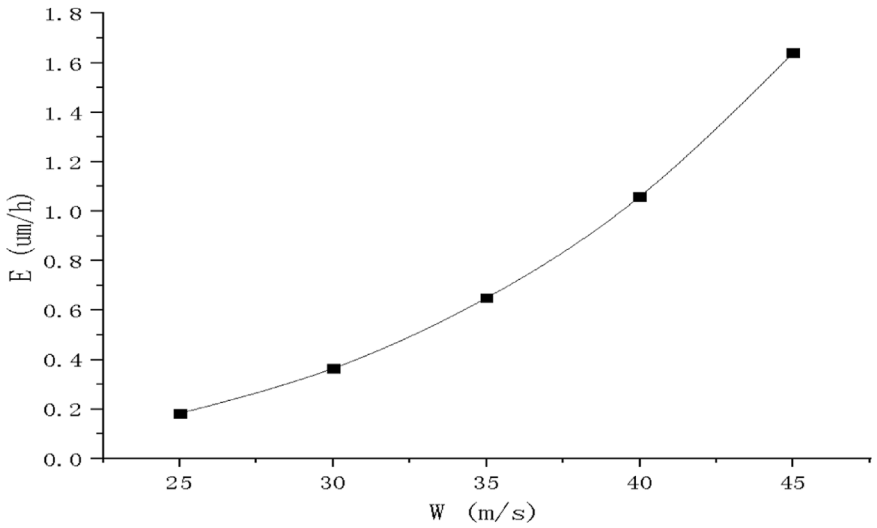

FIGURE 8
Wear amount per unit time.

$$\Delta H = K \cdot S \cdot W^N \cdot T$$

The relationship between material wear and speed is determined by measuring the material wear, as shown in the following Figure 7.

The values of the parameters E and W in the following table are adjusted and calculated, and the coefficient K and the velocity index N are obtained. The results of the adjustment of the measured values are shown in the following Table 4 and in Figure 8.

From Table 4 and Figure 8, There is a good exponential relationship between wear rate and velocity, and the index N is about 3.7. According to material wear curve for wear estimation, namely material test sediment wear curve can be expressed as:

$$\Delta H = 0.65 \times 10^{-9} S \cdot W^{3.7} \cdot T$$

4 Numerical calculation results

4.1 Flow characteristics inside flow channel

The flow characteristics of sediment-laden water largely determine the operational performance of the hydropower station (Li et al., 2020), which in turn affects the wear characteristics of the flow components in the hydropower station. In this regard, flow velocity and sediment distribution are the most important factors affecting wear. First, the flow characteristics within the hydropower station are analyzed under rated operating conditions. As shown in the Figure 9, the pressure gradient is highest in the Spiral casing due to the conversion of potential and kinetic energy of water, followed by the guide vane, stay vane and runner The lowest point of unit pressure is near the runner outlet. At the same time, the flow velocity at the inlet side of the runner in the flow channel is the highest, followed by the outlet side of the runner, and the flow velocity at the rear end of the draft tube is the lowest.

From the distribution of sediment under the above operating conditions in the flow channel, it is evident that sediment is concentrated on the surface of the spiral casing, stay vane, guide vane, turbine blade, draft tube and other flow components, especially on the stay vane and guide vane. The sediment distribution is obviously concentrated on the inlet side of the guide vane, and the outlet side of the back pressure surface of the long vane is also the area with the largest concentration of sediment distribution. When the operating conditions, sediment particle size and sediment concentration change, the phenomenon of concentrated sediment distribution at the above locations does not change significantly. Figure 10.

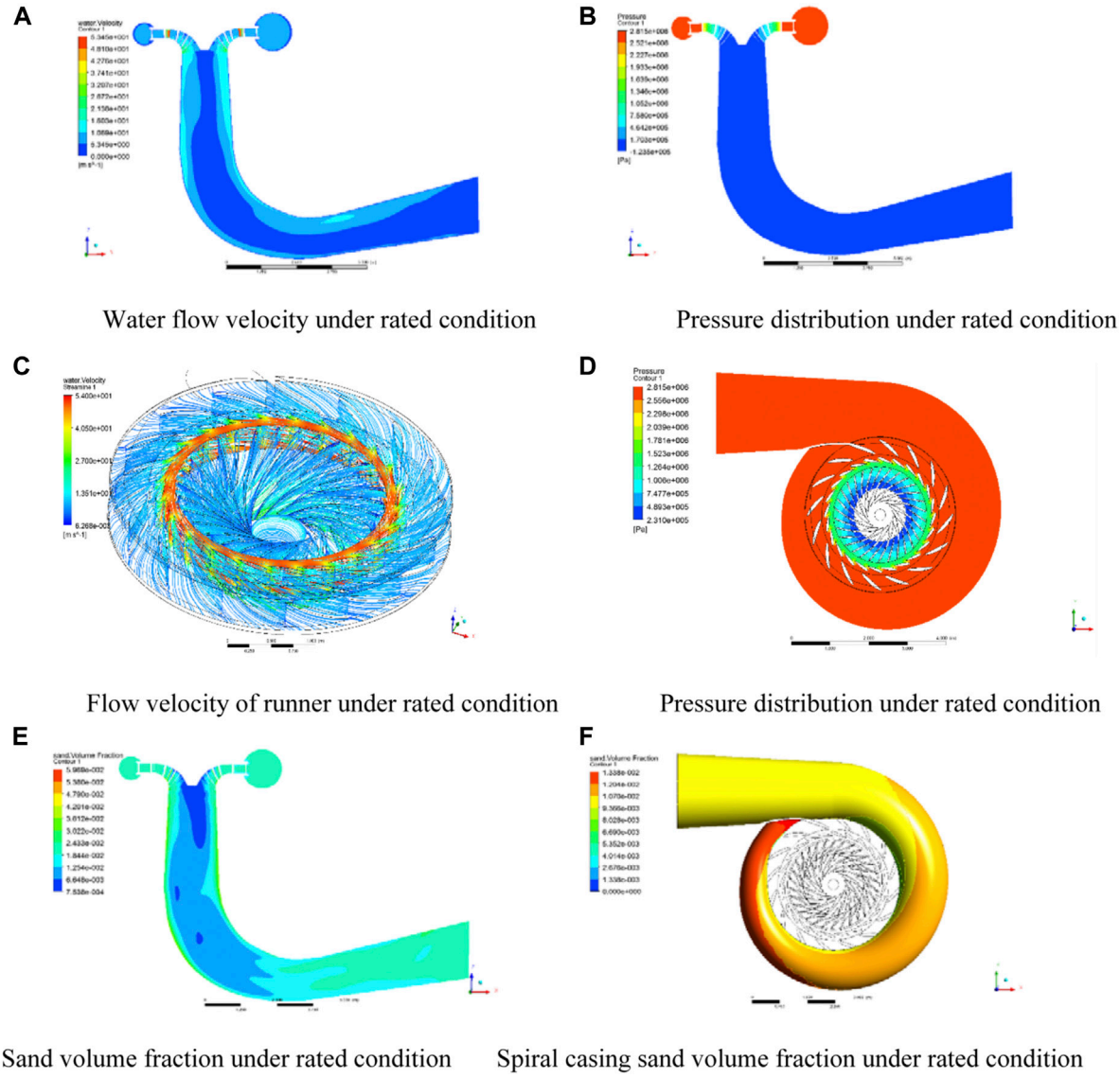

FIGURE 9
Numerical simulation results. **(A)** Water flow velocity under rated condition **(B)** Pressure distribution under rated condition **(C)** Flow velocity of runner under rated condition **(D)** Pressure distribution under rated condition **(E)** Sand volume fraction under rated condition **(F)** Spiral casing sand volume fraction under rated condition.

4.2 Analysis of wear inside the runner

The wear pattern of the water turbine is closely related to sediment distribution and flow velocity (Jiarui, 2021). The distribution of sediment throughout the flow field and the local flow velocity determine which parts and areas of the turbine are more susceptible to wear, which provides a basis for the future design of turbine wear protection. Therefore, the change in sediment distribution and internal flow field characteristics in the flow field will result in different wear conditions in different regions of the turbine (Gao et al., 2002). The material test sediment wear curve obtained by the sediment wear experiment of hydraulic turbine materials is introduced into the simulation calculation. The simulation results are shown in the Figure 11, the sediment sample adjustment formula applied to the simulation calculation of the rated operating conditions after 2,483.92 h determines the amount of wear of each component. The position of the long blade that is susceptible to wear is located near the blade inlet and the outlet of the back pressure surface.

The following conclusions can be drawn: the maximum wear point of the positive pressure surface and the back pressure surface of the long blade~-1.196–1.092 ≈-2.28 mm.

5 Measured results after operation

5.1 Measured results

Unit 3F of a hydropower station began a 72-h trial operation in December 2017. Since its official commissioning, a total of

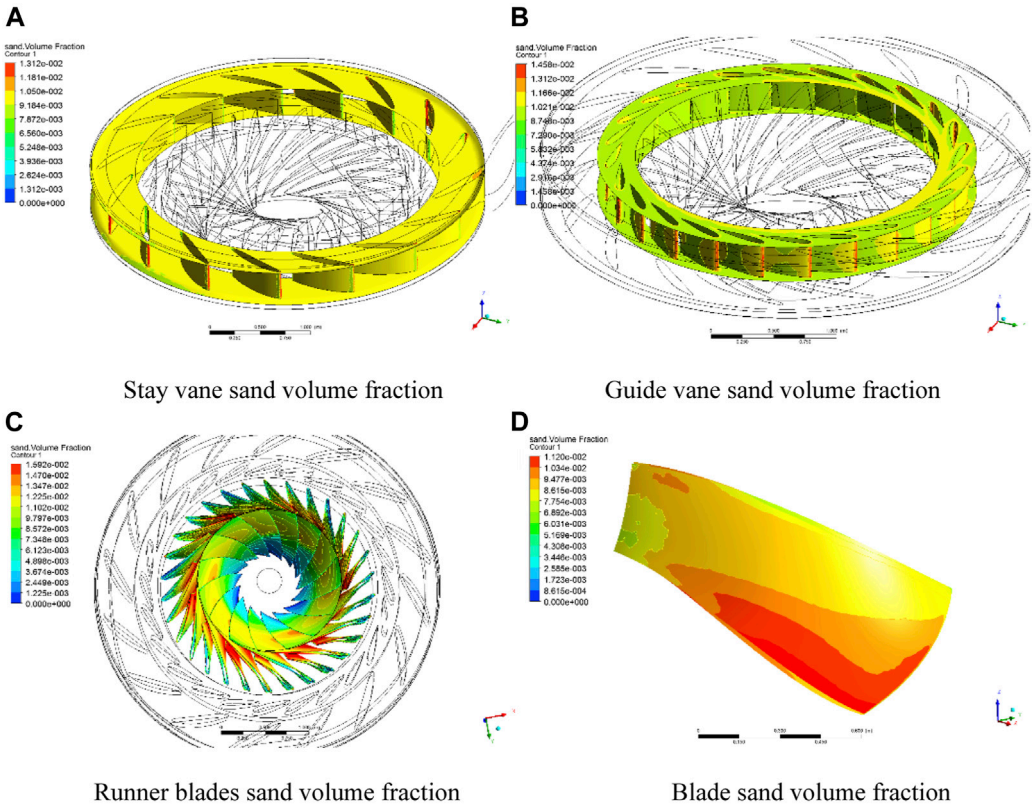

FIGURE 10
Numerical simulation results under rated condition. **(A)** Stay vane sand volume fraction **(B)** Guide vane sand volume fraction **(C)** Runner blades sand volume fraction **(D)** Blade sand volume fraction.

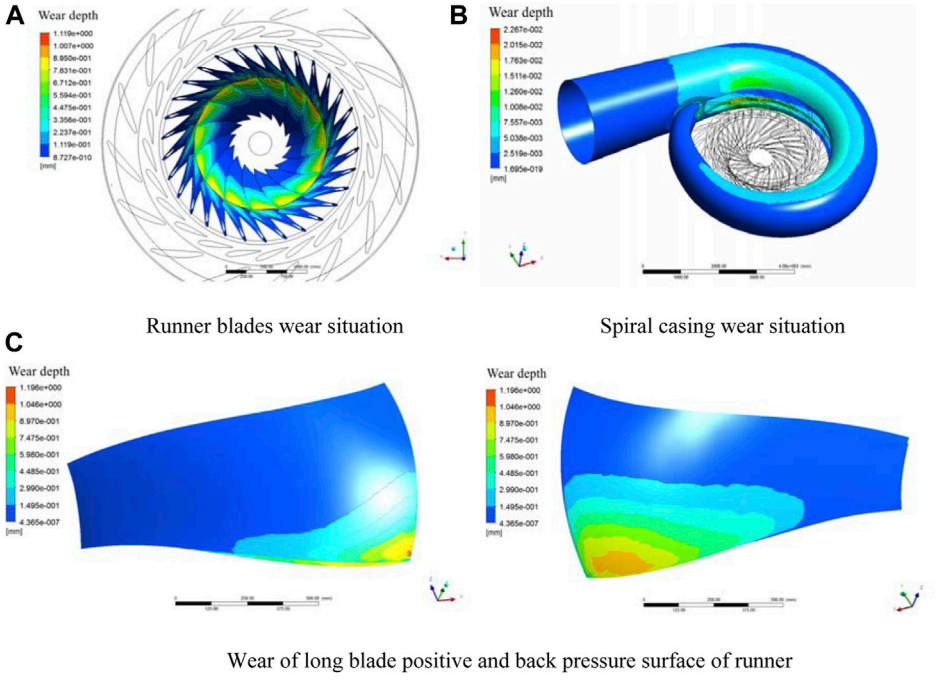

FIGURE 11
Numerical simulation results under wear situation. **(A)** Runner blades wear situation **(B)** Spiral casing **(C)** wear situation Wear of long blade positive and back pressure surface of runner.

FIGURE 12
Measuring point of ultrasonic thickness gauge for turbine blades.

TABLE 5 Theoretical thickness of 1 # blade.

	Theoretical thickness of 1 # blade (mm)			
—	A	B	C	D
a	5.65	8.59	11.48	14.33
b	5.61	8.5	11.34	14.13
c	5.58	8.4	11.19	13.93
d	5.55	8.32	11.05	13.74
e	5.51	8.23	10.91	13.55
f	5.49	8.15	10.78	13.38

TABLE 6 Measured thickness of 1 # blade.

	Measured thickness of 1 # blade (mm)			
—	A	B	C	D
a	3.58	6.56	9.5	12.33
b	4.6	7.58	9.94	12.46
c	4.85	7.64	10.53	13.22
d	5.11	7.58	10.27	13.34
e	4.88	7.71	10.41	13.69
f	5.13	7.76	10.63	13.52

2,483.92 operating hours have been performed. The flow passage and flow components of the unit 3F were inspected. The inspection revealed that the runner edges of the turbine generator of hydropower unit 3F are heavily worn. There are 15 long blades with different degrees of wear on the water edge. Measuring point for measuring blade thickness (Cheng and Chen, 2009) with ultrasonic thickness gauge (Yang, 2020) is shown in Figure 12.

TABLE 7 Thickness and theoretical deviation of 1 # blade.

	Thickness and theoretical deviation of 1 # blade (mm)			
—	A	B	C	D
a	-2.07	-2.03	-1.98	-2.00
b	-1.01	-.92	-1.4	-1.67
c	-.73	-.76	-.66	-.71
d	-.44	-.74	-.78	-0.4
e	-.63	-.52	-0.5	.14
f	-.36	-.39	-.15	.14

5.2 Data analysis and comparison

The data in Table 5 below are the theoretical thickness of each measuring point of runner blade of 3F unit of a hydropower station:

The data in Table 6 below are the existing thickness of each measuring point of runner blade after the 3F unit of a hydropower station operates for 2,483.92 h:

The data in Table 7 below are the difference between the theoretical thickness of runner blades of 3F unit of a hydropower station and the existing thickness of each measuring point after 2,483.92 h of operation:

The results show that after 2,482.92 h of unit operation, the runner of 3F unit was severely worn and the blade thickness was significantly reduced. After measuring the wear of long blades (1#) with ultrasonic thickness gauge, it is found that the wear of blades at A-a position is -2.07 mm, and the predicted wear depth is -2.28 mm according to simulation calculation, with an error of 10.14%.

6 Conclusion

1) In the sediment wear test, the sample material of hydraulic turbine blade is 0Cr13Ni5Mo. Suspended sediment was sampled from the river near the dam of the hydropower station. In the test, the conservative maximum sediment concentration of 1.93 kg/m^3 was taken during the operation of the hydraulic turbine unit. According to the sediment wear test results of five groups of samples at different flow velocities, under the same sediment concentration and sediment composition, the wear depth per unit time of turbine blade material samples increases rapidly with the increase of sand and water velocity.
2) The maximum wear depth of the runner blade in the actual measurement of the unit is -2.07 mm, which is located near the water outlet edge of the runner long blade and the lower ring welding point. The wear depth of the same position predicted by the sediment wear digital simulation for the same operation time cycle is -2.28 mm. The trend of the sediment wear depth of the runner blade is consistent with the actual measurement trend of the unit, and the error of the maximum wear depth prediction is about 10%, Therefore, the digital simulation prediction method has certain engineering guiding significance.
3) The sediment abrasion depth curve obtained by sediment abrasion test, combined with two-phase flow digital simulation calculation based on Euler-Euler equation and turbulence model, can realize conservative prediction of sediment abrasion depth of hydraulic turbine blades, provide a method for flow body design and evaluation of sediment abrasion resistance performance of high head and high sediment concentration hydraulic turbine runner blades, and help to improve the sediment abrasion prevention and control technology of this type of hydraulic turbine blades, And carry out application and promotion in the project.
4) This study also has the following shortcomings: first, it is unable to fully consider all the operating conditions of the turbine runner blades in the complex working environment, as well as the continuous changes of river sediment (Cao et al., 2018) with the upstream water flow. Secondly, the influence of cavitation and sediment coupling on the prediction of runner blade wear depth cannot be considered. At present, we can only measure the maximum sediment concentration with conservative rivers for many years to ensure that there is enough margin for predicting the sediment wear depth of turbine runner blades.

Data availability statement

The original contributions presented in the study are included in the article/Supplementary Material, further inquiries can be directed to the corresponding author.

Author contributions

JP JM, JH, and YZ contributed to the conception and design of the study. YZ and WZ organized the database. JH and JM performed the statistical analysis. JP wrote the first draft of the manuscript. LW and JM performed the finite element calculation. All authors contributed to manuscript revision, and read and approved the submitted version.

Funding

This research was funded by Special Support Plan for High Level Talents in Zhejiang Province (No. 2021R52036).

Conflict of interest

LW was employed by Hangzhou Resource Power Equipment Co. Ltd.

The remaining authors declare that the research was conducted in the absence of any commercial or financial relationships that could be construed as a potential conflict of interest.

Publisher's note

References

Bohn, B., Khoie, R., Gopaluni, R. B., Olson, J. A., and Stoeber, B. (2019). Development and characterization of a non-intrusive sensor to measure wear in centrifugal pumps. *IEEE sensors J.* 19 (18), 7906–7914. doi:10.1109/jsen.2019.2919283

Cao, H., Zhang, J., Dong, X., and Chen, C. (2018). Study on sediment characteristics of baihetan hydropower station [J]. *People's Yangtze River* 49 (23), 16–20. doi:10.16232/j.cnki.1001-4179.2018.23.003

Cheng, L., and Chen, H. (2009). Feasibility analysis on measurement research of turbine blade abrasion of Three Gorges Hydropower Station [J]. *China Water Transp. (the second half of the month)* 9 (12), 105–106. doi:10.3969/j.issn.1006-7973-C.2009.12.054

Gao, Z., Zhou, X., Zhang, S., and Lu, L. (2002). Three dimensional turbulent flow calculation and wear prediction of turbine runner [J]. *Journal of Hydraulic Engineering* 9, 37–43. doi:10.3321/j.issn:0559-9350.2002.09.007

Jiarui, C. (2021). *Study on the relationship between river turbidity of Yingxiuwan Hydropower Station and sediment wear of turbine runner blades [D]*. China: Xihua University. doi:10.27411/d.cnki.gscgc.2021

Li, Y., Guo, B., and Xiao, Y. (2020). Numerical study of hydro-abrasive erosion in high-head Francis turbine runner [J]. *Journal of Hydroelectric Engineering* 39 (02), 112–120. doi:10.11660/slfdxb.20200211

Noon, A. A., and Kim, M. H. (2016). Erosion wear on centrifugal pump casing due to slurry flow. *[J]. Wear* 364-365, 103–111. doi:10.1016/j.wear.2016.07.005

Shi, B., Pan, J., Wu, L., Zhang, X., Qiu, Y., and Zhang, Y. (2020). A prediction method of wear for volute casing of a centrifugal slurry pump. *[J]. Geofluids* 2020, 1–12. doi:10.1155/2020/8847087

Tang, C., Yang, Y. C., Liu, P. Z., and Kim, Y. J. (2021). Prediction of abrasive and impact wear due to multi-shaped particles in a centrifugal pump via CFD-DEM coupling method. *Energies* 14, 2391. doi:10.3390/en14092391

Tao, Y., Bai, Y. M., and Wu, Y. C. (2021). Influence of blade thickness on solid–liquid two-phase flow and impeller wear in a ceramic centrifugal slurry pump. *Processes* 9 (8), 1259. doi:10.3390/pr9081259

Tarodiya, R., and Gandhi, B. K. (2019). Numerical simulation of a centrifugal slurry pump handling solid-liquid mixture: Effect of solids on flow field and performance. *Adv. Powder Technol.* 30, 2225–2239. doi:10.1016/j.apt.2019.07.003

Tian, W. (2020). *Study on internal flow and wear of turbine guide vane in Francis turbine of multi-sediment high head.* China: Xihua University. doi:10.27411/d.cnki.gscgc.2020.000455

Xu, B., Lin, Z., Zhu, Z., and Yu, T. (2022). Experimental and simulation study of the effect of gravity on the solid-liquid two-phase flow and erosion of ball valve. *Advanced Powder Technology* 33, 103416. doi:10.1016/J.APT.2021.103416

Yang, Y. (2020). *A thousand weeks Research on* in situ *ultrasonic thickness measurement technology based on dry coupling [D].* China: Zhejiang University. doi:10.27461/d.cnki.gzjdx.2020.003941

Yu, J., Tang, S., and Pan, L. (2007). "Prediction and analysis of silt wear of xiluodu hydraulic turbine [C]," in *Proceedings of the technical seminar on the stability of hydraulic turbine generator units (AIP)* (Economic Daily Press), 339–347.

Zhou, W., Chai, J., Xu, Z., Cao, C., Wu, G., and Yao, X. (2022). Numerical simulation of solid-liquid two-phase flow and wear prediction of a hydraulic turbine high sediment content. *Experimental Techniques* 2022, 1–13. doi:10.1007/S40799-021-00542-5